Barcelona '10

F018

Beyond the Dots in the Box - Microseismicity-constrained Fracture Models for Reservoir Simulation

S. Williams-Stroud (Microseismic Inc.), L. Eisner (Microseismic Inc.), A. Hill (Microseismic Inc.), P. Duncan* (Microseismic Inc.) & M. Thornton (Microseismic Inc.)

SUMMARY

Monitoring of induced microseismic events usually results in locations for these events and a geometrical interpretation of these dots in the box . In this study we show how additional information obtained from observed microseismic events, namely the source mechanisms, were used to generate a discrete fracture network. Both volumetric and shear-only source mechanism inversion was carried out on microseismic events from the treatment of a shale gas reservoir in the continental US. The source mechanisms revealed fracture orientations more accurately than could be inferred from microseismic event locations alone. The activity associated with different mechanisms is interpreted as indicating reactivation of existing fractures in the rock, as well as suggesting generation of new fractures. Failure analysis using source mechanisms on individual events allows an integrated understanding of the complex fracture interactions taking place in the reservoir, and also provides a more complete understanding of the stress conditions in the reservoir during the treatment. Fracture orientations, locations, and failure mechanisms are translated into discrete fracture network (DFN) models that can be used to verify the extent and character of the fractures created or reactivated during the fracture treatment, and may ultimately be used to generate fracture flow properties for reservoir simulation.

Introduction

Monitoring of seismic events induced by completions and production processes has been increasingly used to develop and optimize oil and gas production. Such monitoring uses microseismic events caused by stress changes in the rock. These stress changes can be caused by various reservoir activities such as hydraulic fracturing, water injection or fluid extraction. The majority of recent applications exploit location analysis of the induced microseismic events. However, the recorded seismic waveforms carry additional information on the mechanism of failure for each of these events. The mechanisms of these events can be used to estimate stress changes instead of inferring these changes from the spatial distribution of the located microseismic events. In this study we show how the source mechanisms of the observed microseismic events were used to differentiate between microseismic events induced on pre-existing faults and those originating from induced hydraulic fracturing. The characterization of micro-seismic events is a key in creating discrete fracture network (DFN) models that can be used to condition models that simulate reservoir production.

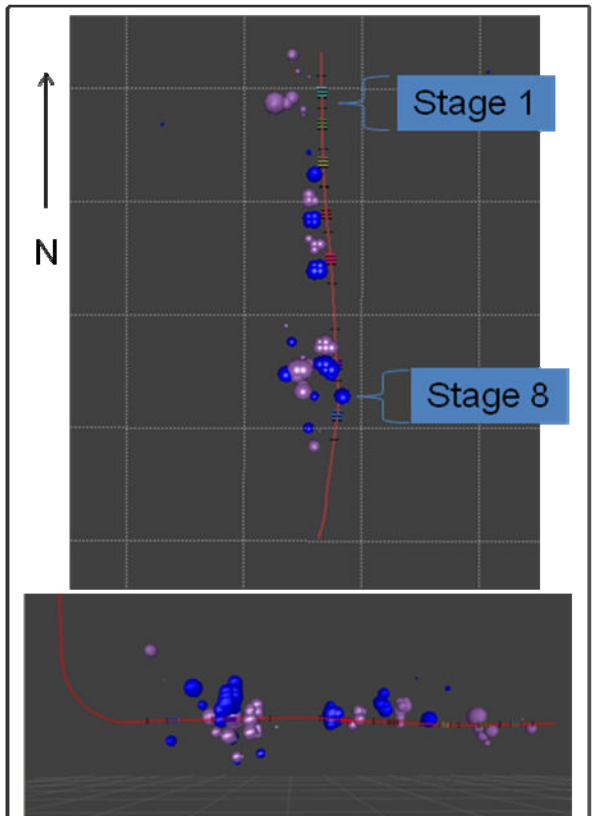

Figure 1 *Map view and vertical cross-section through mapped locations of the microseismic events in this case study. Two types of microseismic events are color-coded: Blue spheres correspond to locations of the reverse faulting events and purple spheres correspond to locations of dip-slip events. Sphere size is proportional to the released seismic moment, the largest sphere (stage 8) represents 9.3 10^9 Nm. Treatment well trajectory is represented by the red line. The induced events are predominantly located west of the treatment well. Dip-slip events are located at the depth of the treatment well while reverse mechanism show significant vertical growth.*

Method

We use source mechanism inversion from the surface data based on a least squares inversion of the observed P-wave amplitudes recorded on the vertical component. The inversion algorithm uses the same data to obtain the full moment inversion (i.e. including the volumetric part of the source mechanism), and double-couple (shear) mechanism. In both cases we assume a point source. The moment tensor representing the source mechanism can be inverted from a point source relationship between observed displacements on vertical component A and moment tensor components M_{jk}:

$$A = G_{3j,k} M_{jk} \ , \qquad (1)$$

Where $G_{3j,k}$ are vertical components of the Green's function derivative (Aki and Richard, 1980). Einstein's summation rules over j,k indexes applies. Equation (1) can be inverted by either least squares (Sipkin, 1982) or a grid search (grid search is possible only for pure shear source mechanism as non-shear source mechanisms have an infinite number of possible combinations of M_{jk}).

Although in principle it is possible to use multiple waves observed at the surface (such as P- and S-waves), only amplitudes of direct P-waves on vertical receiver components are used for inversion of moment tensor in this study as they provide a robust inversion result independent of the poorly constrained S-wave velocity model . The Green's function derivatives of a homogeneous isotropic medium with correction for free surface and attenuation can be written as:

$$G_{3j,k} = \frac{M_0}{4\pi\rho r c^3}\gamma_3\gamma_j\gamma_k 2e^{-\frac{\pi r f}{cQ}}, \qquad (2)$$

here ρ is density, r is the distance between source and receiver, c is P-wave velocity, γ_i are components of a unit vector from source to the receiver, f is dominant frequency of the signal and Q is attenuation coefficient. The exponential term in equation (2) accounts for attenuation and is equal to 1 if attenuation is neglected. The factor of 2 before the exponential term approximates the free surface reflection as the observed waves are both direct and reflected P-waves (i.e., assuming no P-to-S conversion at the free surface). The linear distance r dependence of the moment represents spherical divergence.

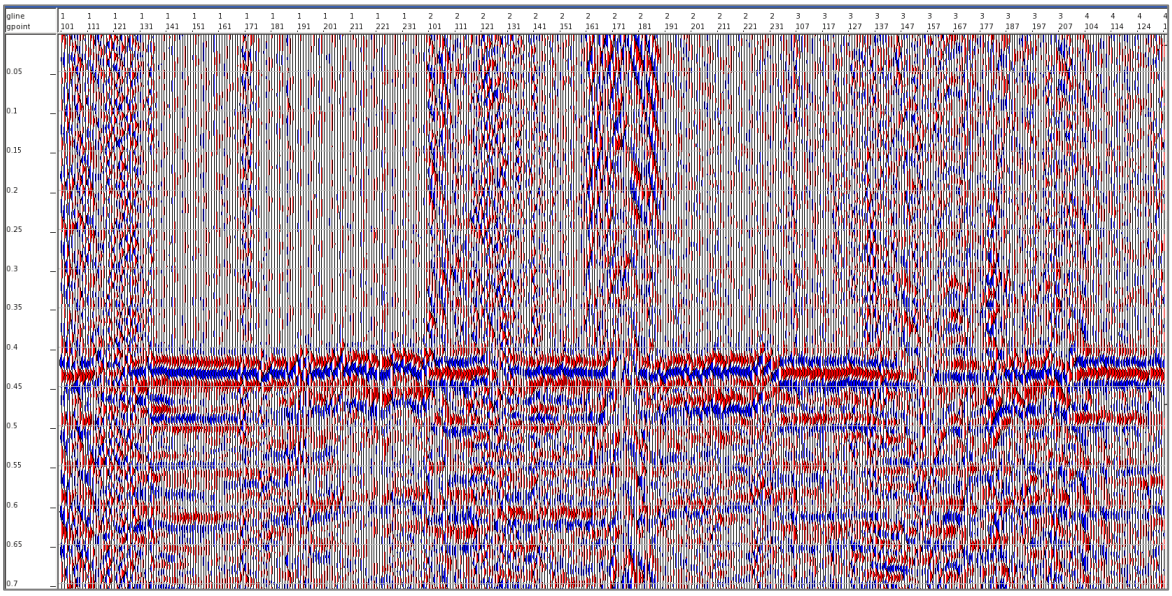

Figure 2 *Move-out corrected sections of the vertical component first arrivals of the largest microseismic event detected in this case study. This event shows polarity change across the spread.*

Case Study

Source mechanisms have allowed us to understand the complex patterns of event locations induced by hydraulic fracture stimulation on a well drilled in the continental USA. This stimulation was performed on a well at an approximate depth of 6,000 ft. Eight treatments of nearly two million barrels of brine with proppant stimulated approximately 4,000 ft of horizontal well section. Average treating pressure was 6,186 psi, average treating rate was 64.7 bpm. The maximum surface pressure reached (during treatment) was 7,845 psi. The microseismic monitoring was carried out with a star-like surface array (FracStar®) consisting of 9 lines 4,000-7,000 ft long. The surface monitoring array consisted of 980 single vertical component receiver stations laid out with approximately 1:1 offset to depth ratio in a star-like pattern. Figure 1 shows map view and vertical cross-section of the located microseismic events that were induced in all fracturing stages. While this dataset shows good signal-to noise quality, the resulting locations are difficult to interpret as fracture trends. There seems to be upward vertical growth of events with a reverse mechanism, as the majority of these events occur above the treatment well. Most of the induced microseismic events are located west of the treatment well suggesting strongly asymmetric hydraulic fractures.

By picking the amplitudes and polarities of the first arrivals shown in Figure 2, maps were generated that show the relative amplitudes and polarity of the P-wave signal for four representative events (Fig. 3). Green symbols on the maps represent upward first motion, red symbols represent downward first motion, and the relative amplitudes of the direct P-waves are represented by the circle size. Receivers without a reliable P-wave pick are not shown in these plots. Note that both size and polarity of the direct arrivals are smoothly varying with distance indicating both consistencies of the picks as well as good consistent coupling of the geophones. The mechanism in the top left plot in Figure 3 represents dip-slip along a vertical fault plane striking 70° NE, with the northern half moving up. The bottom left plot represents dip-slip along a vertical fault plane striking 80° NE with the northern half moving down. Both of the plots on the right side of Figure 3 represent the same mechanism in two different locations beneath the array- reverse faulting with slip along 45° and 50° dipping faults plane striking 70° NE.

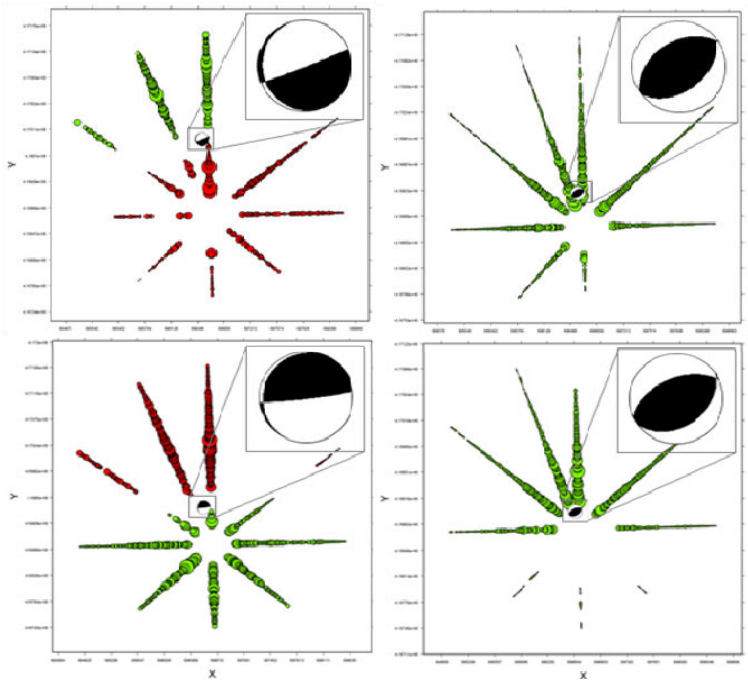

Figure 3 *Map views of polarity and relative sizes of first arrivals for three types of microseismic events induced in this case study. Red circles represent motion down, green circles represent motion up, circles are proportional to relative sizes of the observed amplitudes. The black-and-white beach balls are plotted at the microseismic event epicenters as lower hemisphere projections of the inverted shear components of the general source mechanisms, with an enlarged beach ball in the upper right corner of each plot to show details of the failure mechanism.*

The four source mechanisms shown in Figure 3 represent pure-shear components of the general source mechanisms, that is, the double-couple component of the inverted full moment tensor. For each event of Figure 3 the pure shear components of the general mechanisms account for more than 90% of the released moment. To verify this observation we have also inverted the same datasets restricting the source mechanism to pure shear faulting with an arbitrary orientation and we compared the least-squares misfit between observed data and predicted synthetic amplitudes. The small difference between the misfit of the pure shear and the general mechanism shows that the pure shear mechanisms satisfactorily explain the observed data and non-shear components most likely result from mismodeling and noise. The ability to test the shear-only component is important in the case of the reverse mechanism because a generalized inversion resulted in a large non-shear component but the more simple shear mechanism also explains the data equally well for this event. In other surveys, non-shear mechanisms were found to provide a significantly better fit to the observed data. Note, that each source mechanism inversion has a non-unique solution that results in two possible planes for the pure shear mechanism since slip motion along the two possible planes explains the observed data equally well.

Discrete fracture modeling and source mechanisms

In addition to the conceptual validation that is possible by visualizing a three-dimensional discrete fracture network (DFN) represented by the microseismicity, modeling the flow behaviour of the stimulated reservoir can be facilitated with such models. Properties such as fracture permeability, fracture porosity and fracture connectivity can be calculated from the DFN and used to populate reservoir simulation grids. Figure 4 shows a fracture network constrained by the event locations and mechanisms previously discussed. Fracture size is poorly constrained by wellbore and reflection seismic data attributes, but by using the seismic moment of the events, a reasonable estimate of fracture size per event can be made. The largest fractures in Figure 4 have dimensions consistent with a magnitude 0.7 event based on observations of small induced reservoir earthquakes, such as those analyzed by Tomic et al, 2009. For a given magnitude, the surface area and slip distance are inversely related, but they can both be further constrained by using measured rock rigidity values. The DFN model is based on possible fracture sizes, rather than subjective guesses based only on something that looks reasonable to a geoscientist. Through this analysis, we used the mechanism to interpret differences between microseismic events induced on pre-existing natural faults and events possibly due to new fracture creation. This identification allows us to differentiate between various trends observed in microseismic locations which would be otherwise considered just a 'cloud of dots in a box'.

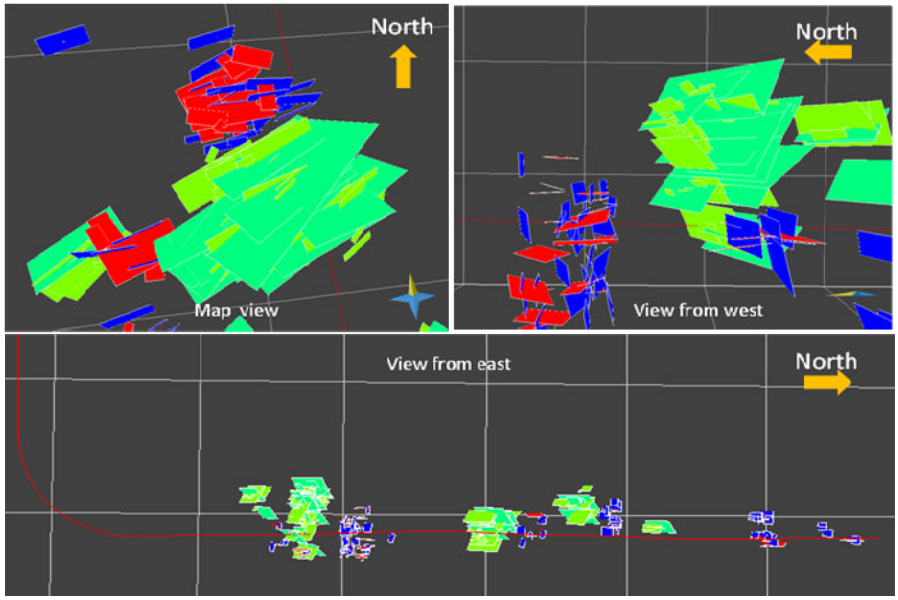

Figure 4 *Discrete fracture network generated from microseismic event locations and inverted source mechanisms. Top left picture is a map view; green and turquoise colored fractures on the reverse failure mechanism planes. Right top picture shows vertical view looking from the west, displaying fracture planes representing the horizontal fractures (red) and associated dip slip fracture planes (blue). In bottom picture, fracture from all frac stages are displayed along the wellbore lateral; view is from the east.*

Acknowledgements
Authors are grateful to the operators for giving permission to show the case study dataset. We also greatly benefited from discussions and help of our many colleagues, particularly Michael Grealy, Shibaji Chatterjee, Julia Kurpan, Dave Abbott and Peter Morton.

References
Aki, K., and Richards, P. G., 2002, Quantitative Seismology, University Science Books, Sausalito, CA.
Tomic, J., Abercrombie, R. E., and do Nasciemento, A. F., 2009, Source parameters and rupture velocity of small M < 2.1 reservoir induced earthquakes, Geophysical Journal International, vol. 179, no. 20, pp. 1013-1023.
Sipkin, S.A., 1982: Estimation of earthquake source parameters by the inversion of waveform data: synthetic waveforms, Phys. Earth planet. Inter., 30, 242-259.